Case Studies in Thermal Engineering 39 (2022) 102461

Contents lists available at ScienceDirect

Case Studies in Thermal Engineering

journal homepage: www.elsevier.com/locate/csite

Heat transfer and friction factor correlations development for double pass solar air heater artificially roughened with perforated multi-V ribs

Varun Pratap Singh [a], Siddharth Jain [a], Ashish Karn [a], Gaurav Dwivedi [b], Ashwani Kumar [c], Sachin Mishra [d], Naveen Kumar Sharma [e], Mohit Bajaj [f,g], Hossam M. Zawbaa [h,i,*], Salah Kamel [j]

[a] Department of Mechanical Engineering, School of Engineering, University of Petroleum and Energy Studies, Energy Acres, Bidholi, Dehradun, Uttarakhand, 248007, India
[b] Energy Centre, Maulana Azad National Institute of Technology, Bhopal, 462 003, India
[c] Technical Education Department Uttar Pradesh, Kanpur, India
[d] School of Electronics and Electrical Engineering, Lovely Professional University, Phagwara, Punjab, India
[e] Electrical Engineering Department, I. K. G. Punjab Technical University, Jalandhar, India
[f] Department of Electrical Engineering, Graphic Era (Deemed to be University), Dehradun, 248002, India
[g] Department of Electrical and Electronics Engineering, National Institute of Technology, Delhi, 110040, India
[h] Faculty of Computers and Artificial Intelligence, Beni-Suef University, Beni-Suef, Egypt
[i] Technological University Dublin, Dublin, Ireland
[j] Electrical Engineering Department, Faculty of Engineering, Aswan University, 81542, Aswan, Egypt

ARTICLE INFO

Keywords:
Solar energy
Solar air heater
Double pass
Artificial roughness
Correlation
Perforation

ABSTRACT

Thermo-hydraulic performance of a Double Pass Parallel Flow Solar Air Heater (DPPFSAH) roughened with perforated multi-V ribs has been studied experimentally in a prior study and the effect of variation in open area ratio and change in relative roughness width has been analysed and reported. The current work builds upon the aforementioned earlier study by discussing in detail the methodology and various steps involved in the development of a correlation for variable parameters with Nusselt number and friction factor for DPPFSAH. The outcomes show that perforations in the multi-V ribs lead to a considerable rise in the Nusselt number, a 9.66 times increase in the thermo-hydraulic performance parameter and nearly a four times increase in friction factor compared to multi-V ribs with smoothed walls. Empirical correlations for the Nusselt number and friction factor were obtained for the double pass parallel flow solar air heater with perforated multi-V ribs established with ±14% and ±7%.

* Corresponding author. Technological University Dublin, Dublin, Ireland.
E-mail addresses: ray_varun@yahoo.com (V.P. Singh), arthjain2001@gmail.com (S. Jain), akarn@ddn.upes.ac.in (A. Karn), gdiitr2005@gmail.com (G. Dwivedi), drashwanikumardte@gmail.com (A. Kumar), rite2sm@gmail.com (S. Mishra), naveen31.sharma@gmail.com (N.K. Sharma), mohitbajaj@nitdelhi.ac.in (M. Bajaj), hossam.zawbaa@gmail.com (H.M. Zawbaa), skamel@aswu.edu.eg (S. Kamel).

https://doi.org/10.1016/j.csite.2022.102461
Received 4 July 2022; Received in revised form 28 September 2022; Accepted 30 September 2022
Available online 1 October 2022

Nomenclature

Symbols

A	Unit area, (m^2)
C_d	Coefficient of discharge
D_h	Duct hydraulic diameter, (m)
e	Rib elevation, (m)
H	Duct elevation (each side), (m)
$\dot{m}$	Mass-flow rate, (kg/s)
W	Duct width, (m)
w	One set rib width, (m)
I	Iradiation (W/m^2)
p	Pitch

Subscripts:

d	Duct/channel, diameter
h	Height, hole
m	mean
u	Useful
s	Smooth

Dimensionless parameters:

Ah/Ar	Relative area
e/Dh	Relative roughness height
f	Duct friction
P/e	Relative roughness pitch
W/H	Duct aspect ratio
Nu	Nusselt Number

Greek symbols:

ΔP	A pressure drop, (Pa)
ηth	Thermal efficiency
ρ	Air density, (kg/m3)
β	Open area ratio
α	Angle of attack (^{o})

Abbreviations:

DPPF	Double Pass Parallel Flow
THPP	Thermo-Hydraulic Performance Parameter
LTS	Low Temperature Systems
SAH	Solar Air Heater

1. Introduction

Solar energy has always been the primary and pre-eminent energy source in terrestrial space and majorly contributed to the renewable domain compared to hydro, wind, geothermal, and biofuel [1–4]. The two primary types of solar energy include solar photovoltaic, which converts sunlight directly into electricity using PV arrays, and solar z technology, which collects the sun's heat for further applications [5]. Solar thermal energy systems can further be classed into three groups based on the temperature of the working fluids: "Low-Temperature Systems (LTS) (up to 150 °C), Medium-Temperature Systems (MTS) (150 °C–400 °C), and High-Temperature Systems (HTS) (greater than 400 °C)" [6]. One of the typical low-temperature systems is a Solar Air Heater (SAH) that gathers radiant energy irradiation to deliver it to an operational medium. SAH is useful; therefore, its multiple benefits, namely convenient structure, cheaper construction, small-pressure difference, single-phase working fluid, corrosion-free structure and being an almost static type of device. SAH is employed all over the world for low-temperature gradient applications such as paddy and fruit drying, timber drying, cash crop drying, water heating, agricultural season extension, pre-heating, process heating, workplace ventilation, makeup air, air conditioning, space heating, and cooling, etc. [7]. However, two primary challenges associated with SAH are handling large volumes of air and inadequate thermal characteristics among airflow and the roughened base plate. Many researchers have proposed several design solutions with varied roughness shapes to enhance SAH thermo-hydraulic performance (THP) [8].

Variations in structural elements, roughness variables, and the number of flow passages seem to be the most common strategies explored by researchers to boost systems thermo-hydraulic performance parameter (THPP) [9]. As the use of Double Pass Solar Air

Heater (DPSAH) provides more collection surface and distance for the working fluid to move within, it offers a significant improvement in thermal performance [10]. The configurations that are used as the key variables that affect the effectiveness of a DPSAH include parallel-flow [11,12], cross-flow [12–14], and recycling or circular-flow [13].

The study of DPSAH comprises: theoretical and numerical analysis, exergy and energy analysis and empirical studies to find out the THP and effectiveness of the applied method [17]. To improve the THP of DPSAH, investigators applied porous media, packed bed [18], thermal energy storage media [19] and created artificial roughness through extended surfaces like fins [11], wedges [20], baffles [21], vertex generators [22], turbulators [23], winglets [24], wire mesh [18], and ribs [25].

For multiple-V shaped ribs, Hans et al. [26], Lanjewar et al. [27], Singh et al. [28–30] and Sharma et al. [31] and for staggered V ribs, Jin et al. [32] select the optimal configuration for variable combinations. For perforated V-blockages over continuous blockages, Alam et al. [33] observed gains in THP and Nusselt number (*Nu*) of 50% and 33%, correspondingly, and a reduction in friction factor (*f*) value of 32%. Perforated V-baffles enhance *Nu* by a factor of 1.5–3, according to Chamoli and Thakur [34]. Skullong et al. [20] employed rectangular and trapezoidal perforated-winglets with vortex generators (WVGs) and found improvements in *Nu, f*, and *THP* of 7.1, 109.5, and 1.84 times and 6.78, 84.32, and 2.01 times above the flat plate, respectively.

Sopian et al. [35] studied DPSAH with porous and non-porous media and found the thermal performance of the DPSAH was about 60–70% higher compared to a smooth channel. Hassan et al. [13,15] inquire about the V-corrugated shape and found an improvement of 71.85% in THP over a smooth SAH. For the same flow conditions, Yeh et al. [16] examined the parallel flow (PF) SAH with fins attached to the absorber plate and detected an increase in performance. Ravi and Saini [36] discovered that the DPSAH positively affected the Nu/Nu_s by 3.4 times and the f/f_s by 2.5 times when compared to a single pass SAH (SPSAH). Ravi and Saini [37] also developed "correlations for forced convective type counter flow solar air heater having discrete multi-V shaped and staggered rib roughness on both sides of the absorber plate."

Multiple research groups established thermodynamic relationships for SAH in order to obtain the optimum possible combination of roughness configurations and their characteristics [38]. Early on, "a mathematical model and a solution procedure for predicting the thermal performance" was suggested by Ong [39]. Sharma et al. [10] established a correlation for "double-pass solar air heater having V-shaped ribs roughness". Saini and Saini [40] constructed *Nu* and *f* correlations for arc-type geometry rib roughness and observed a 3.8-fold and 1.75-fold improvement in *Nu* and *f*. Varun et al. [41,42] established a correlation for SPSAH for *Nu* and *f* with ±14% and ±7% accuracy, respectively. Sethi et al. [43] found a link between artificially roughened SAH and dimpled form roughness, as well as reporting a considerable gain in *THP* values. Hans et al. [26] established a correlation for multiple-v type ribs, with the highest *Nu* and *f* values achieved as 6 and 5 times greater when compared to the smooth channel. The optimum thermal performance was observed at a $W/w = 6$, while the optimum *f* was found at $W/w = 10$ at $\alpha = 60°$. For high flow rates, Hernández and Quinonez [44] noticed that double-pass parallel flow SAH (DPPFSAH) is better than double-pass counter flow SAH (DPCFSAH) so far as the air does not really gain much useful energy by circling beneath the base plate.

There are a limited number of investigations that have explored the impact of variance in open area ratio (β) on SAH performance. The influence of the perforations on the flow characteristics has been studied in several ways, including full-half perforated shapes [45], perforation circularity [46], and proportion of open area ratio (β), hole position [47]. Both the open area ratio (β) and the re-circulation time have a significant effect on SAH THP [63].

According to a review, the application of DPPFSAH produces minimal drag forces, resulting in low pumping power and good heat transfer efficiency [44]. Due to the high fluid velocity of the secondary flow induced by perforations, perforation enhances the performance of SAH [17,48]. DPPFSH with perforations in multi-V ribs roughness may have a significant impact in enhancing *Nu* and lowering *f* due to the high flow velocity across auxiliary routes. Singh et al. [30] previously conducted experiments for multi-V ribs with perforation in single and double pass SAH and demonstrated an appreciable rise in *Nu, f* and *THPP* values when compared to unbroken multi-v ribs and smooth channels. In consideration of the above, the current work explores the methodology and various steps involved in the development of a correlation for variable parameters with *Nu* and *f*.

Table 1
Parameters value and range for DPPFSAH.

Parameter Notation with Unit	Value
W	0.3 m
H	0.025 m
W/H	12
D_o/D_p	0.55
D_h,	0.04615 m
e	0.002 m
e/D	0.043
p/e	10
α	60 ^{o}
W/w	2: 2:10
β	0.0, 0.21, 0.27, 0.31
Re	2000:2000:18,000
I	800 W/m^2
Rib shape	Multi-V

2. Setup configuration

The detailed description of the setup, roughness configuration, parameter range and governing equations are already discussed in previous work done by Varun et al. [30] and shown in Table 1. A DPPFSAH duct having multi-V ribs roughness geometry examined in this study is shown in Fig. 1 (a) to (d), is constructed as per the ASHRAE standard (AHSRAE 93–77, 1977) [49].

3. Data handling and setup validation

A detailed methodology of data collection, governing equations, validation and error analysis was reported in a prior work by

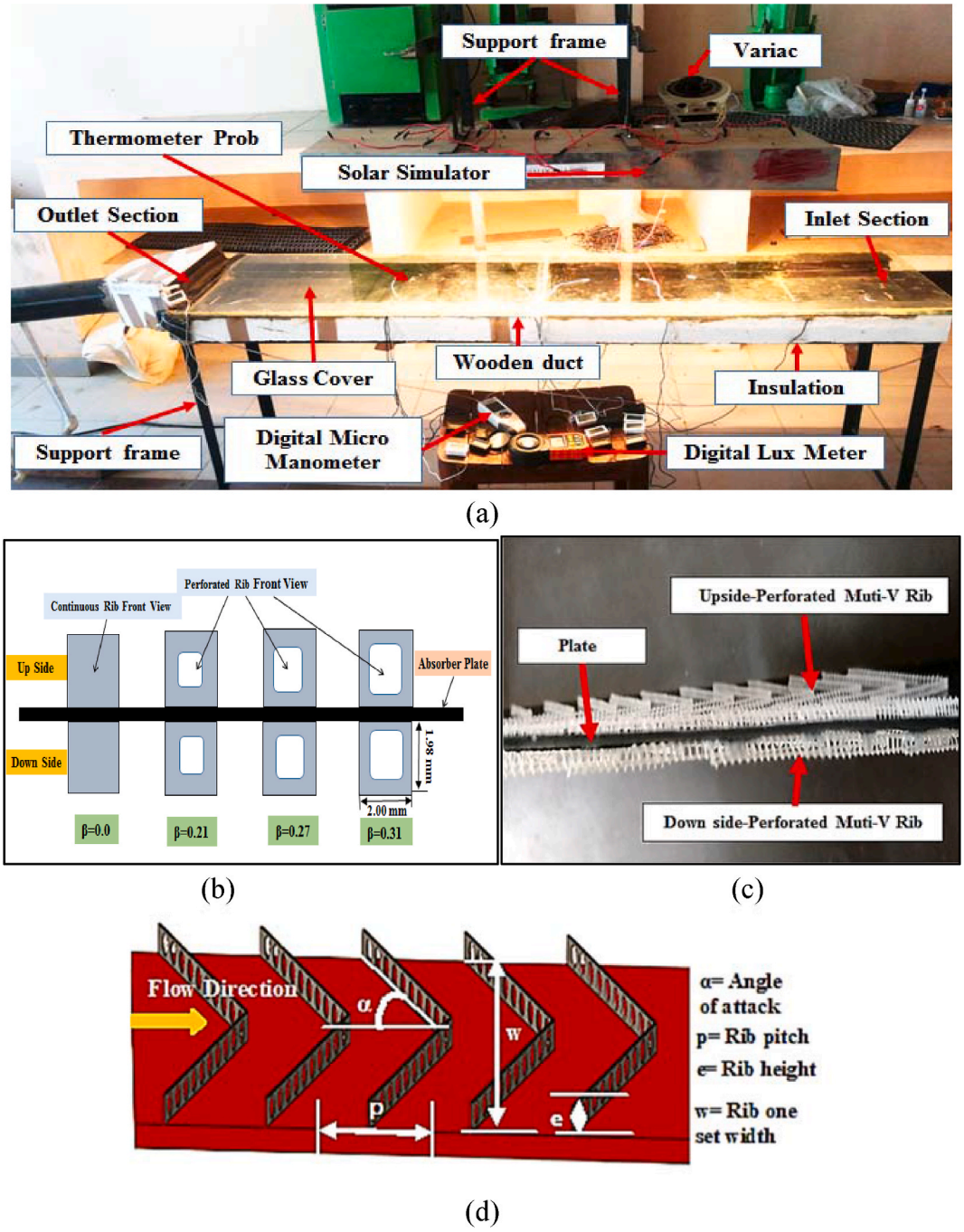

Fig. 1. (a) Experimental setup with (b) Front illustration of ribs with varying open area ratios and (c) Absorber plate with perforated-V ribs on both side of plate and (d) orientation of plate in DPFSAH [30].

Table 2
Typical set of roughness (system) parameters.

Plot No.	*W/w*	*(β)*	*P/e*	*W/H*	*α*	*e/D*
1.	2	0.21	10	12	60°	0.043
2.	4	0.27	10	12	60°	0.043
3.	6	0.31	10	12	60°	0.043
4.	8		10	12	60°	0.043
5.	10		10	12	60°	0.043

Varun et al. [30]. The *Nu* and *f* readings were used to evaluate the coefficients of the Dittus-Boelter and Blasius equations, respectively, in an experimental set-up [26].

The Modified Dittus-Boelter equation becomes:

$$Nu_s = 0.024 Re^{0.8}\, Pr^{0.4} \tag{1}$$

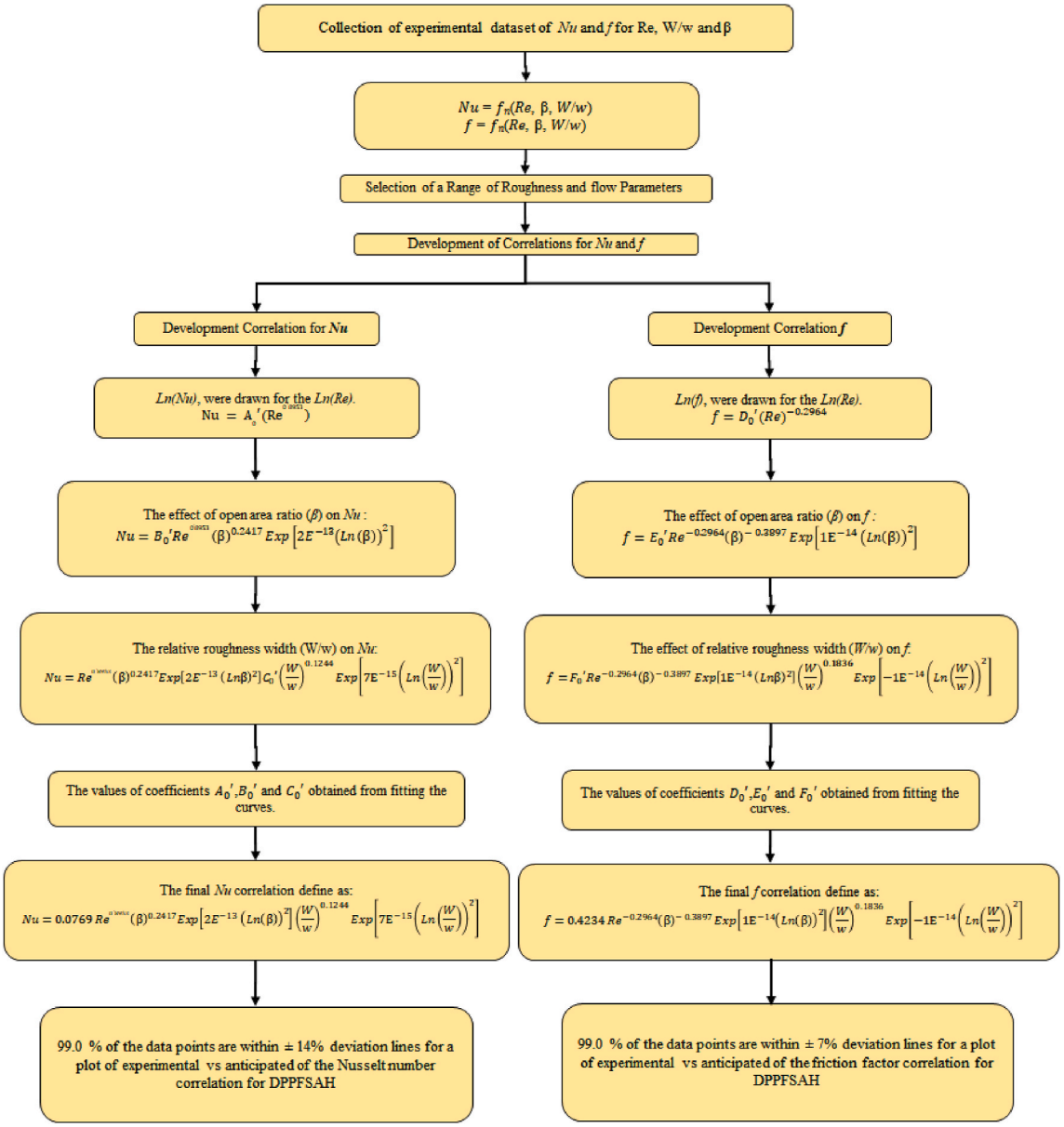

Fig. 2. Steps of correlation methodology.

and the modified Blasius equation takes the form:

$$f_s = 0.085Re^{-0.025} \tag{2}$$

For error analysis, the present study uses the Kline and McClintock [50] method. Singh et al. [30] have previously discussed the details of the steps required for identifying uncertainty for a range of parameters. The mean % errors in *Nu*=±1.86 %, *Re*=±1.69 % and $f = \pm 3.29$ %, respectively.

The thermal performance, THPP, of multi-V ribs with perforations in DPPFSAH is examined and assessed in relation to design and operating ribs specifications. Detailed descriptions of the effects of the operating parameters like *Re*, *W/w* and β on thermo-hydraulic performance was analysed in a consecutive work performed by Singh et al. [30].

4. Methodology

For DPPFSAH, the assumptions which are under consideration includes quasi-heat transfer modes, uniform heat-flux distribution along the duct; conductive heat transfer from glass to both sides of absorber plate and convective heat transfer within the duct [51,52]. To simplify the analysis and mathematical modeling governing equations assumptions considered incompressible-turbulent flow conditions, uniform temperature distribution within three-dimensional flow maintaing quasi-static state with air leak-proof and perfectly insulated test section. To determine the relationship between *Nu* and *f* with different design and operational paramenters, a set of statistics for a specific range of fixed and variable parameters is presented in Table 2. A detailed steps of correlation methodology have been discussed in below mentioned Fig. 2.

5. Correlations for *Nu* and *f* for DPPFSAH

To establish the *Nu* and *f* correlations, the DPPFSAH functional connection has been established for each set of data of *Nu* and *f* values, which are directly dependent on ribs architecture and geometrical parameters [40], i.e. *Re, W/w*, and β. For parameters in the ranges of β = 0.21–0.31, *W/w* = 2–10, and *Re* = 2000–18000, the correlation is valid. *Nu* and *f* have the following functional relationships:

$$Nu = (\mathrm{Re}, \beta, \mathrm{W/w}) \tag{3}$$

$$\mathrm{f} = (\mathrm{Re}, \beta, \mathrm{W/w}) \tag{4}$$

The present functional relationship excludes the Prandtl number because of an extra factor of ~0.87 on the Nusselt number. The correlation is developed at a constant Prandtl number and therefore assumed its effect is negligible. And if fluids with different Prandtl numbers are considered then the effect on the Nusselt number must also be reconsidered.

5.1. Correlation for Nusselt number (Nu)

Correlations are used to indicate the variation in a parameter's numeric value in relation to other variables. As an outcome, the following expression is employed to calculate the *Nu* correlation:

- *Nu* increases in a consistent manner, as Re increases,
- *Nu* attained optimum value at *W/w* = 6, for the entire range of W/w values,

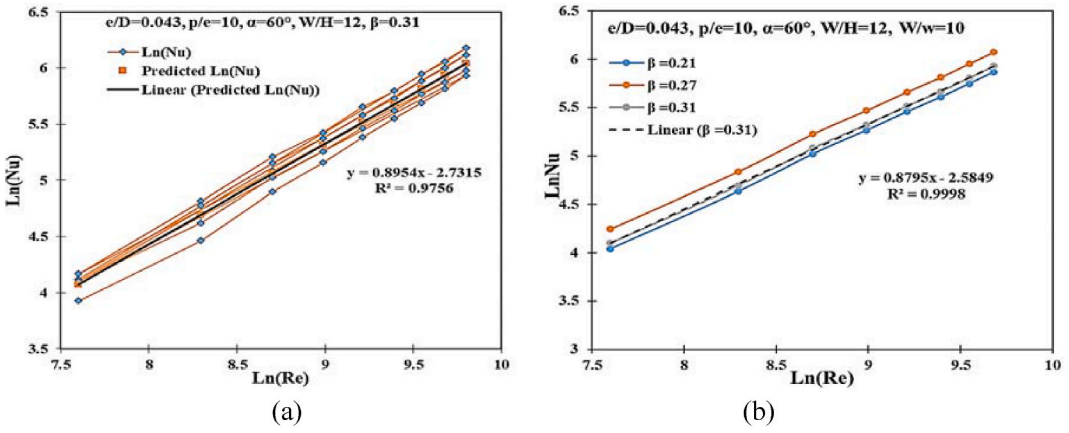

Fig. 3. Graph of Ln (*Nu*) vs. Ln (Re) to calculate the "A_0"' and slop "n"' for different sets of W/w and β in DPPFSAH.

$$Ln(Nu) = Ln\left(A_0^{'}\right) + n^{'}\ Ln(Re) = A_1^{'} + n^{'}\ Ln(Re) \tag{5}$$

- *Nu* attained optimum value at $\beta = 0.27$, for the entire range of open area ratio (β).

Fig. 3 (a) and (b) shows that the results of the experiment provide continuous smooth lines with reasonably regular slopes (n') and the highest variance of 3.28 %, whereas the intercept (A_0') of every line presents a broad variety for the highest divergence of 35.24 %. For the different configurations of roughness geometric parameters, namely W/w and β, the corresponding graph of the Ln (*Nu*) vs. Ln (*Re*) has been shown. The trend of the curve inside the graph of Ln (*Nu*) vs. Ln (*Re*) can be represented for equation (3).

Eq. (5) can alternatively be expressed as follows:

$$Nu = A_0^{'} Re^{n^{'}} \tag{6}$$

Where $A_0^{'} = exp(A_1^{'})$

Fig. 4 (a) shows, the least square method application to generate the best fit curve for the complete range of datasets associated with twenty-one unique sets of roughened absorber plates, and the resulting connection may be represented as follows:

$$\mathrm{Nu} = \mathrm{A}_0^{'}\left(\mathrm{Re}^{0.8953}\right) \tag{7}$$

$$Ln\left[\frac{Nu}{\mathrm{Re}^{0.8953}}\right] = Ln\left(B_1^{'}\right) + B_2^{'}\, Ln(\beta) + \mathrm{B}_3^{'}\,[Ln(\beta)]^2 \tag{8}$$

It may be rearranged as follows:

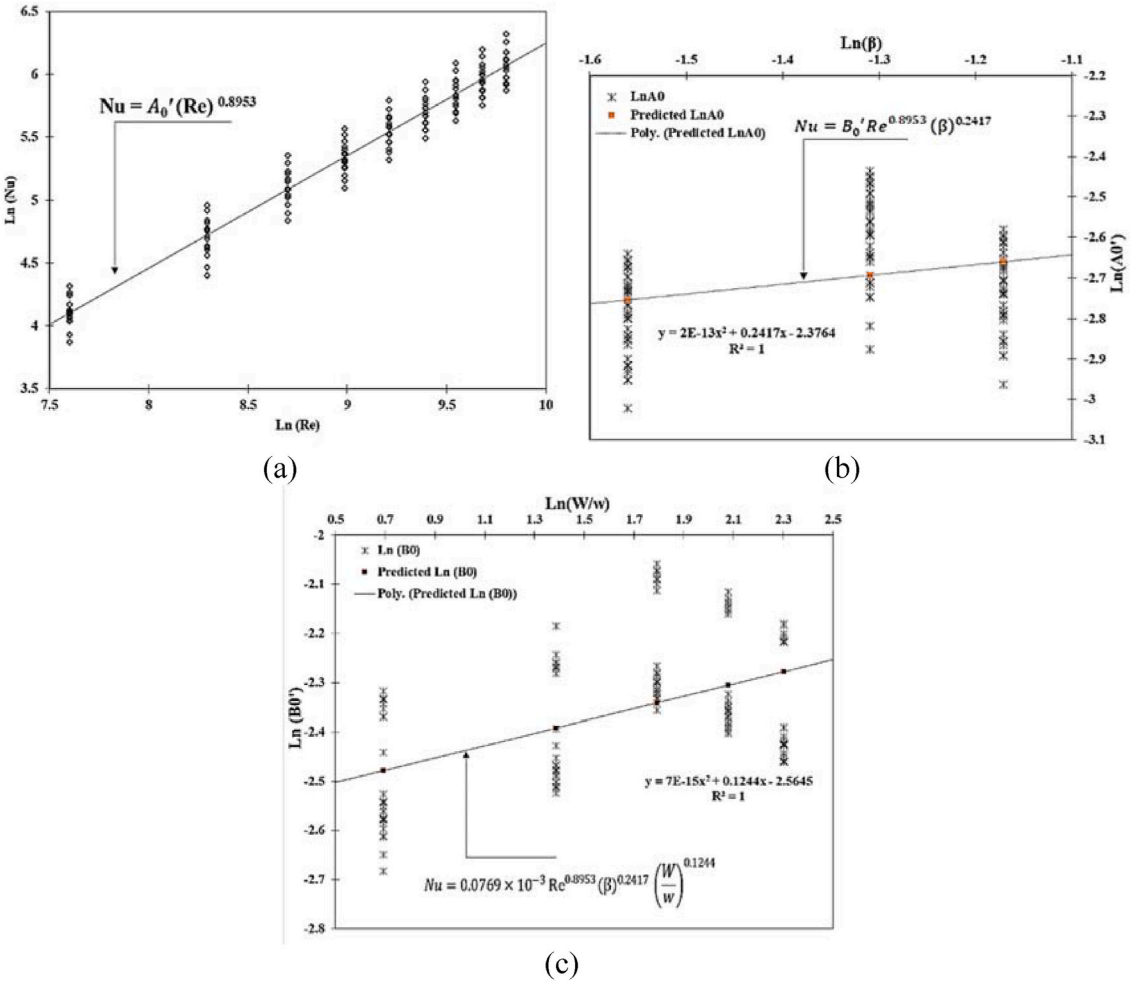

Fig. 4. (a) Ln (*Nu*) vs. Ln (Re), (b) Ln (A_o') vs. Ln (β) and (c) Ln(B_0') vs. Ln(W/w) plot for DPPFSAH.

$$\frac{Nu}{\mathrm{Re}^{0.8953}} = B_0'(\beta)^{B_2'} \exp\left[B_3' (Ln(\beta))^2\right] \tag{9}$$

Where $B_0' = exp(B_1')$

Replacing the curve fitting values for B_2' and B_3' yields the following formulas;

$$\frac{Nu}{\mathrm{Re}^{0.8953}} = B_0'(\beta)^{0.2417} \exp\left[2 \times 10^{-13} (Ln(\beta))^2\right] \tag{10}$$

As for all values of β, $\exp[2 \times 10^{-13}(Ln(\beta))^2] = 1.00$ and can safely be ignored. The value of coefficient B_0' in equation (10) is a product of other contributing factors, specifically W/w and plotting Ln (Nu) and Ln (W/w) for DPPFSAH provides the desired findings. Fig. 4 (b) plots the second-order polynomial relation to representing the optimum curve fitting in order to establish the effective connection in Ln(B_0') and Ln (W/w). In Fig. 4 (c), the results of $B_0' = \frac{Nu}{\mathrm{Re}^{0.8953}(\beta)^{0.2417}}$ has been compared across W/w while addressing the parameter W/w.

To best match the data set, the second order polynomial relation can be produced as:

$$n\left[\frac{Nu}{\mathrm{Re}^{0.8953}(\beta)^{0.2417}}\right] = Ln(C_1') + C_2' Ln\left(\frac{W}{w}\right) + C_3'\left(Ln\left(\frac{W}{w}\right)\right)^2 \tag{11}$$

This may be further simplified as,

$$\frac{Nu}{\mathrm{Re}^{0.8953}(\beta)^{0.2417}} = C_0'\left(\frac{W}{w}\right)^{C_2'} exp\, C_3'\left(Ln\left(\frac{W}{w}\right)\right)^2 \tag{12}$$

Where $C_0' = exp(C_1')$

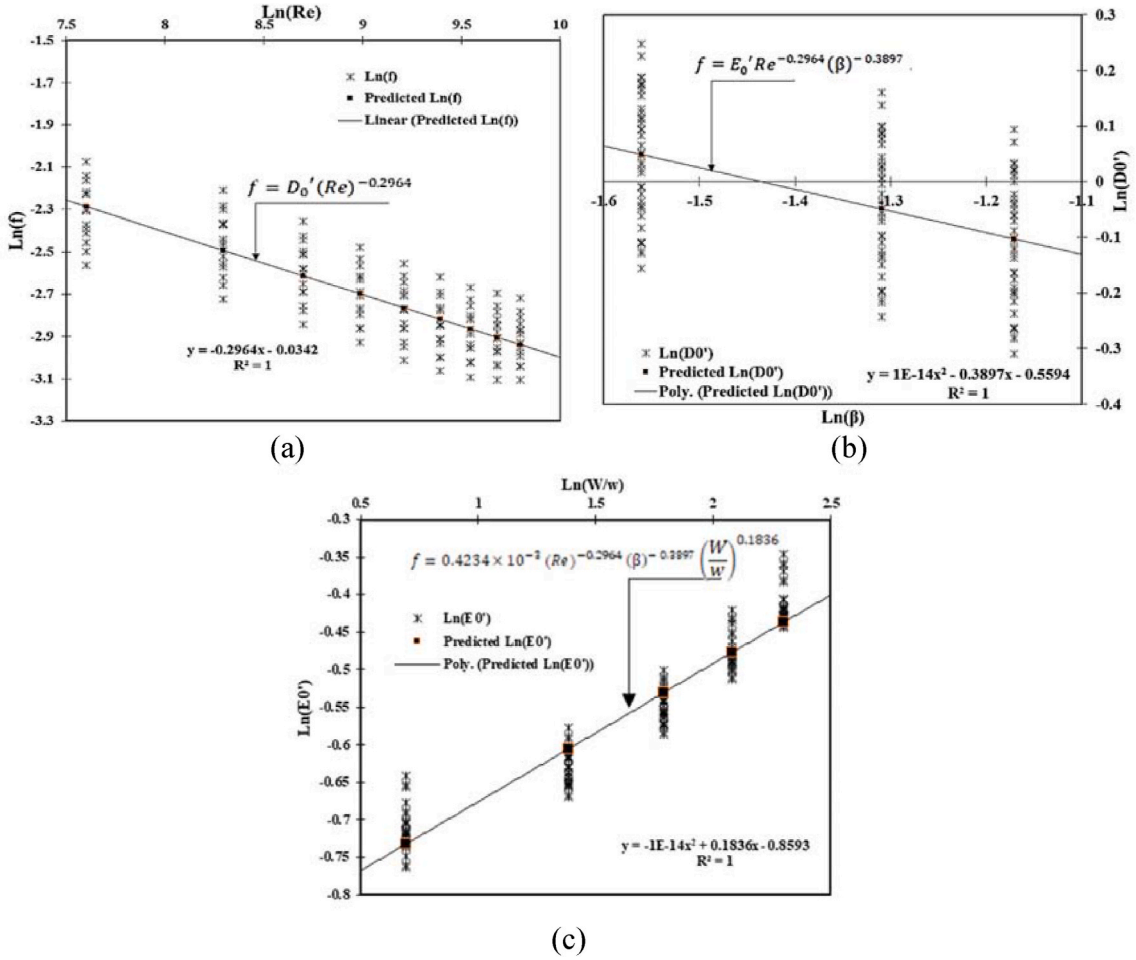

Fig. 5. (a) Ln(f) vs. Ln(Re), (b) Ln(Do') vs. Ln(β) and (c) Ln(E_o') vs. Ln(W/w) plot for empirical data sets of DPPFSAH.

Replacing the quantities of C_2', C_3' generated from the curve fitting regression yields,

$$\frac{Nu}{\mathrm{Re}^{0.8953}(\beta)^{0.2417}} = C_0^{'}\left(\frac{W}{w}\right)^{0.1244} \; exp\left[7\mathrm{E}^{-15}\left(Ln\left(\frac{W}{w}\right)\right)^2\right] \tag{13}$$

As for all values of W/w, $exp\left[7\mathrm{E}^{-15}\left(Ln\left(\frac{W}{w}\right)\right)^2\right] = 1.00$and can be safely ignored.

$$Nu = \mathrm{Re}^{0.8953}(\beta)^{0.2417}\; C_0^{'}\left(\frac{W}{w}\right)^{0.1244} \tag{14}$$

The values of coefficients $A_0^{'} = 0.0670$, $B_0^{'} = 0.0929$ and $C_0^{'} = 0.0769$ for DPPFSAH are the results of curves to be fitted in Fig. 4 (a)–(c).

The resulting *Nu* correlation is as follows:

$$Nu = 0.0769 \times 10^{-3}\; \mathrm{Re}^{0.8953}(\beta)^{0.2417}\left(\frac{W}{w}\right)^{0.1244} \tag{15}$$

5.2. Correlation for friction factor (f)

The correlation for *f* was calculated using the same method as above mentioned for *Nu*. The function for *f*, similar to *Nu*, has been proven to be strongly related to plate geometry design parameters (*W/w* and β) along with flow parameters (*Re*). The following is the influence of different roughness parameters on *f* values:

- The value of *f* decreases uniformly as *Re* increases,
- The value of *f* increases as *W/w* increases, reaching a maximum value of $W/w = 10$,
- As the open area ratio (β) increases, f drops until it reaches a minimum level at $\beta = 0.31$.

The experimental data were used to perform regression analysis, which provides the optimum curve fitting with the intercepts and gradient coefficient to the *f* correlations computation as a function of *Re* can be shown in Fig. 5 (a). Regression analyses were performed on empirically gathered data to generate the following best-fit curve:

$$Ln(f) = Ln\left(D_0^{'}\right) + nLn(Re) = D_1^{'} + nLn(Re) \tag{16}$$

$$f = D_0^{'}(Re)^{-0.2964} \tag{17}$$

Where $D_0^{'} = \exp(D_1^{'})$

The coefficient D_0' for DPPFSAH is the outcome of other contributory components such as β and *W/w*. Fig. 5 (b) represents the effect of values of $D_0^{'} = \frac{f}{(Re)^{-0.2964}}$related to every combinations of open area ratio (β) projected across the perforated multi-V ribs. A regression analysis to adapt a second-order polynomial relation across the data set can be expressed as follows:

$$Ln\left[\frac{f}{(Re)^{-0.2964}}\right] = Ln\left(E_1^{'}\right) + E_2^{'}\,Ln(\beta) + \mathrm{E}_3^{'}\,[Ln(\beta)]^2 \tag{18}$$

It can be rearranged as follows

$$\frac{f}{(Re)^{-0.2964}} = E_0^{'}(\beta)^{E_2^{'}}\,\exp\left[\mathrm{E}_3^{'}\,(Ln(\beta))^2\right] \tag{19}$$

Where $E_0^{'} = \exp(E_1^{'})$

Substituting the values of $E_2^{'}, \mathrm{E}_3^{'}$from the curve fitting results in the following expression;

$$\frac{f}{(Re)^{-0.2964}} = E_0^{'}(\beta)^{E_2^{'}}\; exp\left[\mathrm{E}_3^{'}\,(Ln(\beta))^2\right] \tag{20}$$

Or

$$\frac{f}{(Re)^{-0.2964}} = E_0^{'}(\beta)^{-0.3897}\;\; exp\left[1 \times 10^{-14}\,(Ln(\beta))^2\right] \tag{21}$$

As for all values of β, $exp[1 \times 10^{-14}\,(Ln(\beta))^2] = 1.00$ and can safely be ignored. The coefficient E_0' in equation (21) is the consequence of different influencing parameters, specifically *W/w* values, and the preferred graphs can be acquired through projecting Ln(*f*) vs. Ln(*W/w*) for DPPFSAH. For developing a significant link in-between Ln(E_0') and Ln (*W/w*), the perfect suited curve is described by a second-order polynomial expression. Taking the variables *W/w* into account, the results of $\mathrm{E}_0^{'} = \frac{\mathrm{f}}{(Re)^{-0.2964}\,(\beta)^{-0.3897}}$ were mapped out for different *W/w* values in Fig. 5 (c).

To best match the data, the following second-order polynomial connection was produced.

$$Ln\left[\frac{f}{(Re)^{-0.2964}\ (\beta)^{-0.3897}}\right] = Ln\left(F_1^{'}\right) + F_2^{'}\ Ln\left(\frac{W}{w}\right) + F_3^{'}\left(Ln\left(\frac{W}{w}\right)\right)^2 \tag{22}$$

This may be further simplified as,

$$\frac{f}{(Re)^{-0.2964}\ (\beta)^{-0.3897}} = F_0^{'}\left(\frac{W}{w}\right)^{F_2^{'}} Exp\left[F_3^{'}\left(Ln\left(\frac{W}{w}\right)\right)^2\right] \tag{23}$$

Where $F_0^{'} = \exp(F_1^{'})$

Replacing the values of $F_2^{'}$, $F_3^{'}$ generated from the curve fitting regression provides,

$$\frac{f}{(Re)^{-0.2964}\ (\beta)^{-0.3897}} = F_0^{'}\left(\frac{W}{w}\right)^{0.1836} exp\left[-1\times10^{-14}\left(Ln\left(\frac{W}{w}\right)\right)^2\right] \tag{24}$$

As for all values of W/w, $exp\left[-1\times10^{-14}\left(Ln\left(\frac{W}{w}\right)\right)^2\right] = 1.00$ and can be safely ignored.

$$f = F_0^{'}(Re)^{-0.2964}\ (\beta)^{-0.3897}\left(\frac{W}{w}\right)^{0.1836} \tag{25}$$

The magnitude of coefficients $D_0^{'} = 0.9663$, $E_0^{'} = 0.5715$ and $F_0^{'} = 0.4234$ for DPPFSAH were derived by adapting the contours in Fig. 5 (a)–(c).

The resulting correlation for *f* is as follows:

$$f = 0.4234 \times 10^{-3}\ (Re)^{-0.2964}\ (\beta)^{-0.3897}\left(\frac{W}{w}\right)^{0.1836} \tag{26}$$

5.3. Nu and f deviations between experimental and theoretical dataset

Fig. 6 (a) and (b) compare the experimental and theoretical *Nu* and *f* values and find about 99% of the data sets come under ±14% and ±7% deviation lines, respectively. So, the known correlations equation no. (15) and (26) can be used to anticipate the *Nu* and *f* values inside allowable limits for the variables investigated in the current study.

6. Conclusions

With varied parameters of perforated ribs exposed to constant heat flux, discussion on thermal performance and correlations for *Nu* and *f* values for DPPFSAH reveal that multi-V ribs with perforation offers a considerable gain in thermal outcomes while maintaining relatively low friction losses. The following findings were obtained from the proposed study:

- Multi-V ribs with larger perforations the DPPFSAH improves the recirculation and reattachment zones of fluid flow at the bottom of the rib while lowering flow resistance and improving reattachment intervals, leading to a greater *THP* for the DPPFSAH.

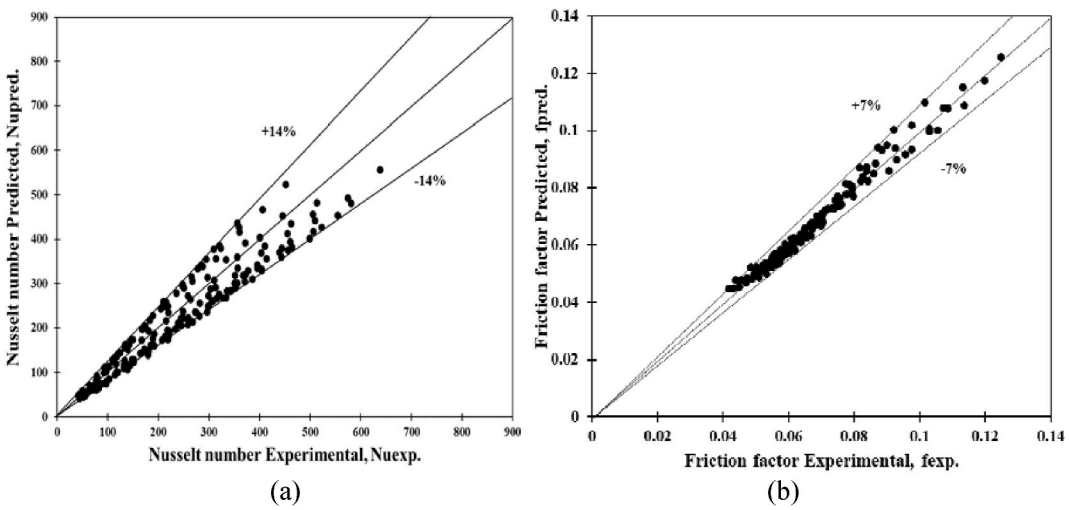

Fig. 6. Comparative between actual and expected (a) *Nu* and (b) f findings for DPPFSAH correlation.

- By enabling flow separation due to secondary pass, perforation reduces the reattachment zone and its length behind the rib, increasing flow mixing and minimizing blower energy requirements.
- Open area ratio (β) = 0.27 was found to be the optimum option across all cases and DPPFSAH with perforation performed better when compared to the smooth channel.
- When compare to smooth duct, the highest increase in *Nu/Nus* and *f/fs* were noticed 9.66 times and 12.31 times, respectively.
- The optimal reading of *THPP* was determined to be 3.96, with an open area ratio (β) = 0.27.
- Correlation for *Nu* and *f* inside acceptable ranges of within ±14% and ±7% deviation lines for the geometry and operational parameters are also developed.

As a novelty of the work, it is the first time the concept of perforation is used in multi-Vrib roughness and a discussion on reattachment zone, the effect of secondary flow and the effect on THPP for optimum value of perforation has been done. The results support the application of perforation, the optimal open area ratio of multi-V ribs with perforation enhances *THP* notably, in contrast to a smooth SAH.

For perforation, optimum values of geometry and operation parameters can be further analysed for different ribs in artificially roughened SAH.

Author statement

Varun Pratap Singh: Conceptualization, Software, Review, Editing, Writing, Original Draft, **Siddharth Jain:** Conceptualization, Software, Review, Editing, Writing, Original Draft, **Ashish Karn:** Investigation, Formal Analysis, Supervision, Writing, **Gaurav Dwivedi:** Investigation, Formal Analysis, Supervision, Writing, **Ashwani Kumar:** Conceptualization, Investigation, Supervision, Writing, **Sachin Mishra:** Conceptualization, Investigation, Supervision, Writing, **Naveen Kumar Sharma:** Supervision, Writing, Review, Editing, **Mohit Bajaj:** Writing, Review, Editing, **Hossam M. Zawbaa:** Writing, Review, Editing, **Salah Kamel:** Supervision, Writing, Review, Editing.

Declaration of competing interest

The authors declare that they have no known competing financial interests or personal relationships that could have appeared to influence the work reported in this paper.

Data availability

Data will be made available on request.

Acknowledgement

The work of Hossam M. Zawbaa was supported by the European Union's Horizon 2020 Research and Enterprise Ireland under the Marie Skłodowska-Curie Grant 847402. The authors thank the support of the National Research and Development Agency of Chile (ANID), ANID/Fondap/15110019.

References

[1] C. Silvi, The use of solar energy in human activities throughout the centuries, Ann. Arid Zone 49 (3–4) (2010) 157–174.
[2] S. Jain, M.P. Sharma, Study of oxidation stability of Jatropha curcas biodiesel/diesel blends, Int. J. Energy Environ. 2 (3) (2011) 533–542.
[3] S. Jain, M.P. Sharma, Engine performance and emission analysis using oxidatively stabilized Jatropha curcas biodiesel, Fuel 106 (2013) 152–156, https://doi.org/10.1016/j.fuel.2012.11.076.
[4] D. Verma, E. Fortunati, S. Jain, X. Zhang, Biomass, Biopolymer-Based Materials, and Bioenergy: Construction, Biomedical, and Other Industrial Applications, first ed., Elsevier Science, 2019.
[5] M. Saini, A. Sharma, V.P. Singh, S. Jain, G. Dwivedi, Solar thermal receivers — a review, Lect. Notes Mech. Eng. II (2022), https://doi.org/10.1007/978-981-16-8341-1, 1_25.
[6] K. Ravi Kumar, N.V.V. Krishna Chaitanya, N. Sendhil Kumar, Solar thermal energy technologies and its applications for process heating and power generation – a review, J. Clean. Prod. 282 (2020), 125296, https://doi.org/10.1016/j.jclepro.2020.125296.
[7] R.L. Webb, E.R.G. Eckert, Application of rough surfaces to heat exchanger, Int. J. Heat Mass Tran. 15 (1972) 1647–1658.
[8] R. P. Saini Varun, S.K. Singal, A review on roughness geometry used in solar air heaters, Sol. Energy 81 (11) (2007) 1340–1350, https://doi.org/10.1016/j.solener.2007.01.017.
[9] H.S. Arunkumar, et al., Review on the design modifications of a solar air heater for improvement in the thermal performance, Sustain. Energy Technol. Assessments 39 (2020), 100685, https://doi.org/10.1016/j.seta.2020.100685. January.
[10] A. Sharma, G. Bharadwaj, Varun, Heat transfer and friction factor correlation development for double-pass solar air heater having V-shaped ribs as roughness elements, Exp. Heat Tran. 30 (1) (2017) 77–90, https://doi.org/10.1080/08916152.2016.1161676.
[11] A. Fudholi, K. Sopian, M.H. Ruslan, Thermal efficiency of double pass solar collector with longitudinal fins absorbers thermal efficiency of double pass solar collector with longitudinal fins absorbers, Am. J. Appl. Sci. (2016), https://doi.org/10.3844/ajassp.2011.254.260 no. March 2011.
[12] N. Kumar, et al., Overview of V-RIB geometries in solar air heater and performance evaluation of a new V-RIB geometry, Renew. Energy 152 (3) (2020) 77–90, https://doi.org/10.1016/j.tsep.2020.100493.
[13] H. Hassan, M.S. Yousef, S. Abo-elfadl, Energy , exergy , economic and environmental assessment of double pass V-corrugated-perforated finned solar air heater at different air mass ratios, Sustain. Energy Technol. Assessments 43 (December 2020), 100936, https://doi.org/10.1016/j.seta.2020.100936, 2021.
[14] R.K. Ravi, R.P. Saini, Effect of roughness elements on thermal and thermohydraulic performance of double pass solar air heater duct having discrete multi V-shaped and staggered rib roughness on both sides of the absorber plate, Exp. Heat Tran. 6152 (1) (2017) 47–67, https://doi.org/10.1080/08916152.2017.1350217.

[15] H. Hassan, S. Abo-Elfadl, Experimental study on the performance of double pass and two inlet ports solar air heater (SAH) at different configurations of the absorber plate, Renew. Energy 116 (2018) 728–740, https://doi.org/10.1016/j.renene.2017.09.047.
[16] C.-D. Ho, Y.-E. Tien, C.-F. Hsiao, The influences of recycle effect on double-pass V-corrugated solar air heaters, Int. J. Green Energy 14 (13) (2017) 1083–1092, https://doi.org/10.1080/15435075.2017.1357123.
[17] T. Alam, M.-H. Kim, A critical review on artificial roughness provided in rectangular solar air heater duct, Renew. Sustain. Energy Rev. 69 (October 2016) 387–400, https://doi.org/10.1016/j.rser.2016.11.192, 2017.
[18] S. Singh, Experimental and numerical investigations of a single and double pass porous serpentine wavy wiremesh packed bed solar air heater, Renew. Energy 145 (2020) 1361–1387, https://doi.org/10.1016/j.renene.2019.06.137.
[19] S.M. Salih, J.M. Jalil, S.E. Najim, Experimental and numerical analysis of double-pass solar air heater utilizing multiple capsules PCM, Renew. Energy 143 (2019) 1053–1066, https://doi.org/10.1016/j.renene.2019.05.050.
[20] S. Skullong, P. Promthaisong, P. Promvonge, C. Thianpong, M. Pimsarn, Thermal performance in solar air heater with perforated-winglet-type vortex generator, Sol. Energy 170 (May) (2018) 1101–1117, https://doi.org/10.1016/j.solener.2018.05.093.
[21] S. Singh, P. Dhiman, Thermal and thermohydraulic efficiency of recyclic-type double-pass solar air heaters with fins and baffles, Heat Tran. Eng. 37 (15) (2016) 1302–1317, https://doi.org/10.1080/01457632.2015.1119619.
[22] B. Kumar, M. Kumar, A.K. Patil, S. Jain, Effect of V cut in perforated twisted tape insert on heat transfer and fluid flow behavior of tube flow: an experimental study, Exp. Heat Tran. 32 (6) (2019) 524–544, https://doi.org/10.1080/08916152.2018.1545808.
[23] A.S. Abdullah, M.M. Abou Al-sood, Z.M. Omara, M.A. Bek, A.E. Kabeel, Performance evaluation of a new counter flow double pass solar air heater with turbulators, Sol. Energy 173 (2018) 398–406, https://doi.org/10.1016/j.solener.2018.07.073.
[24] A. Berber, M. Gürdal, M. Yetimoğlu, Experimental study on the heat transfer enhancement in a rectangular channel with curved winglets, Exp. Heat Tran. (2021) 1–21, https://doi.org/10.1080/08916152.2021.1951897, 00, no. 00.
[25] R. Kumar, V. Goel, S. Bhattacharyya, V. V Tyagi, A.M. Abusorrah, Experimental investigation for heat and flow characteristics of solar air heater having symmetrical gaps in multiple-arc rib pattern as roughness elements, Exp. Heat Tran. (2021) 1–18, https://doi.org/10.1080/08916152.2021.1905752, 0, no. 0.
[26] V.S. Hans, R.P. Saini, J.S. Saini, Heat transfer and friction factor correlations for a solar air heater duct roughened artificially with multiple v-ribs, Sol. Energy 84 (6) (2010) 898–911, https://doi.org/10.1016/j.solener.2010.02.004.
[27] A.M. Lanjewar, J.L. Bhagoria, R.M. Sarviya, Performance analysis of W-shaped rib roughened solar air heater, J. Renew. Sustain. Energy 3 (4) (2011), https://doi.org/10.1063/1.3595740.
[28] V.P. Singh, S. Jain, J. Gupta, Analysis of the effect of perforation in multi-v rib artificial roughened single pass solar air heater: - Part A, Exp. Heat Tran. 35 (6) (Oct. 2021) 1–20, https://doi.org/10.1080/08916152.2021.1988761.
[29] V.P. Singh, S. Jain, J.M.L. Gupta, Analysis of the effect of variation in open area ratio in perforated multi-V rib roughened single pass solar air heater- Part A, Energy Sources, Part A Recover. Util. Environ. Eff. 44 (4) (2022) 1–20, https://doi.org/10.1080/15567036.2022.2029976.
[30] V.P. Singh, S. Jain, J. Gupta, Performance assessment of double-pass parallel flow solar air heater with perforated multi-V ribs roughness — Part B, Exp. Heat Tran. 35 (6) (2022) 1–18, https://doi.org/10.1080/08916152.2021.2019147.
[31] R. Maithani, S. Sharma, A. Kumar, Thermo-hydraulic and exergy analysis of inclined impinging jets on absorber plate of solar air heater, Renew. Energy 179 (2021) 84–95, https://doi.org/10.1016/j.renene.2021.07.013.
[32] D. Jin, J. Zuo, S. Quan, S. Xu, H. Gao, Thermohydraulic performance of solar air heater with staggered multiple V-shaped ribs on the absorber plate, Energy 127 (2017) 68–77, https://doi.org/10.1016/j.energy.2017.03.101.
[33] T. Alam, R.P. Saini, J.S. Saini, Experimental investigation on heat transfer enhancement due to V-shaped perforated blocks in a rectangular duct of solar air heater, Energy Convers. Manag. 81 (2014) 374–383, https://doi.org/10.1016/j.enconman.2014.02.044.
[34] S. Chamoli, N.S.S. Thakur, Correlations for solar air heater duct with V-shaped perforated baffles as roughness elements on absorber plate, Int. J. Sustain. Energy 35 (May 2015) 37–41, https://doi.org/10.1080/14786451.2013.857318, 2013.
[35] K. Sopian, M.A. Alghoul, E.M. Alfegi, M.Y. Sulaiman, E.A. Musa, Evaluation of thermal efficiency of double-pass solar collector with porous – nonporous media, Renew. Energy 34 (3) (2009) 640–645, https://doi.org/10.1016/j.renene.2008.05.027.
[36] R.K. Ravi, R.P. Saini, Experimental investigation on performance of a double pass artificial roughened solar air heater duct having roughness elements of the combination of discrete multi V shaped and staggered ribs, Energy 116 (2016) 507–516, https://doi.org/10.1016/j.energy.2016.09.138.
[37] R.K. Ravi, R.P. Saini, Nusselt number and friction factor correlations for forced convective type counter flow solar air heater having discrete multi V shaped and staggered rib roughness on both sides of the absorber plate, Appl. Therm. Eng. 129 (2018) 735–746, https://doi.org/10.1016/j.applthermaleng.2017.10.080.
[38] V.P. Singh, et al., Recent developments and advancements in solar air heaters : a detailed review, Sustain. Times 14 (19) (2022) 1–57, https://doi.org/10.3390/su141912149.
[39] K.S. Ong, Thermal performance of solar air heaters-Experimental correlation, Sol. Energy 55 (3) (1995) 209–220, https://doi.org/10.1016/0038-092X(95)00027-O.
[40] S.K.K. Saini, R.P.P. Saini, Development of correlations for Nusselt number and friction factor for solar air heater with roughened duct having arc-shaped wire as artificial roughness, Sol. Energy 82 (12) (2008) 1118–1130, https://doi.org/10.1016/j.solener.2008.05.010.
[41] V.P. Singh, S. Jain, A. Kumar, Establishment of correlations for the Thermo-Hydraulic parameters due to perforation in a multi-V rib roughened single pass solar air heater, Exp. Heat Tran. 35 (5) (2022) 1–20, https://doi.org/10.1080/08916152.2022.2064940.
[42] V.P. Singh, S. Jain, A. Karn, A. Kumar, G. Dwivedi, Mathematical modeling of efficiency evaluation of double pass parallel flow solar air heater, Sustainability 14 (17) (2022) 1–22, https://doi.org/10.3390/su141710535.
[43] M. Sethi, Varun, N.S.S. Thakur, Correlations for solar air heater duct with dimpled shape roughness elements on absorber plate, Sol. Energy 86 (9) (Sep. 2012) 2852–2861, https://doi.org/10.1016/j.solener.2012.06.024.
[44] A.L. Hernández, J.E. Quiñonez, Analytical models of thermal performance of solar air heaters of double-parallel flow and double-pass counter flow, Renew. Energy 55 (2013) 380–391, https://doi.org/10.1016/j.renene.2012.12.050.
[45] R. Karwa, B.K.K. Maheshwari, Heat transfer and friction in an asymmetrically heated rectangular duct with half and fully perforated baffles at different pitches, Int. Commun. Heat Mass Tran. 36 (3) (2009) 264–268, https://doi.org/10.1016/j.icheatmasstransfer.2008.11.005.
[46] J.S. Kwak, S. Shin, Effect of hole shape on the heat transfer in a rectangular duct with perforated blockage walls, J. Mech. Sci. Technol. 22 (April) (2008) 1945–1951, https://doi.org/10.1007/s12206-008-0736-7.
[47] S. Chamoli, N.S. Thakur, Heat transfer enhancement in solar air heater with V-shaped perforated baffles, J. Renew. Sustain. Energy 5 (2) (2013), https://doi.org/10.1063/1.4798411.
[48] B. Kumar, A.K. Patil, S. Jain, M. Kumar, Effects of double V cuts in perforated twisted tape insert: an experimental study, Heat Tran. Eng. 41 (17) (2020) 1473–1484, https://doi.org/10.1080/01457632.2019.1649926.
[49] J.E. Hill, ASHRAE 93-97. Standard, method of testing to determine the thermal performance of solar air heater, New York Am. Soc. Heating, Refrig. Air Cond. Eng. 93 (97) (1977) 1–34.
[50] S.J. Kline, The purposes of uncertainty analysis, J. Fluid Eng. 107 (1985) 153–160.
[51] C. Choudhury, P.M.M. Chauhan, H.P.P. Garg, Design curves for conventional solar air heaters, Renew. Energy 6 (7) (1995) 739–749, https://doi.org/10.1016/0960-1481(95)00007-7.
[52] S.A. Klein, W.A. Beckman, J.A. Duffie, A design procedure for solar heating systems, Sol. Energy 18 (2) (1976) 113–127, https://doi.org/10.1016/0038-092X(76)90044-X.